(Received 11 September 2025, Accepted 3 November 2025, Scheduled 11 November 2025)

A New Method for Failure Diagnosis of Programmable Metasurfaces

Fang-Fang Wang[1,*], Wei Cheng[1], Yiqian Mao[2], and Qing Huo Liu[3,4]

[1] *College of Electronic and Optical Engineering Nanjing University of Posts and Telecommunications, Nanjing 210003, China*
[2] *State Key Laboratory of Millimeter Waves, Southeast University, Nanjing 210096, China*
[3] *Eastern Institute of Technology, Ningbo 315200, China*
[4] *Xiamen University, Xiamen 361005, China*

ABSTRACT: In this paper, a new method is proposed for failure diagnosis of programmable metasurfaces, which jointly uses the single-point measurement strategy and Bernoulli-Gaussian (BG) prior. Specifically, leveraging the dynamic tuning property of programmable metasurfaces, the radiated fields is measured with a single fixed probe, therefore reducing the time and error of the measurement process. Moreover, the BG prior inherent in the programmable metasurface under test is exploited during the reconstruction process in order to perform the diagnosis with a small number of measurements without resorting to prior knowledge of the radiation pattern of the failure-free programmable metasurface. The accuracy, efficiency, and robustness of the proposed method are verified through a set of representative numerical experiments, where the results are compared with those from existing diagnostic methods.

1. INTRODUCTION

With their extraordinary ability for electromagnetic manipulation, programmable metasurfaces have been widely adopted in millimeter-wave imaging [1], satellite communications [2], biomedical diagnostics [3], and wireless communications [4]. Typically, programmable metasurfaces consist of massive resonant elements. Due to hardware constraints and deployment environments, however, these resonant elements are likely to fail. Ref. [5] pointed out that about 4.4% of the total number of elements could fail within a year of continuous operation. Such a failure rate will significantly distort the radiation pattern of the programmable metasurface, thereby affecting the overall system performance. Hence, it is critical to diagnose programmable metasurfaces for their effective operation.

In general, such a diagnostic problem can be formulated as a linear inverse one. Unfortunately, to obtain reliable results, traditional linear inversion methods such as the least square (LS) method usually require a large number of measurements, which substantially increases the time cost [6].

According to compressive sensing (CS) theory, the sparsity of the signal can be exploited to reduce the number of measurements required to ensure robust recovery. In fact, the number of faulty resonant elements is usually much smaller than the total number of resonant elements. One may use the differential strategy to take advantage of the sparsity of failures and convert the original diagnostic problem into a sparse signal recovery problem [7–9]. However, employing the differential strategy requires prior knowledge of the radiation pattern of the failure-free programmable metasurface [10, 11]. This will limit the applicability of CS-based diagnostic techniques.

In recent years, deep learning has emerged as a powerful paradigm for failure diagnosis [12]. However, these methods typically require large volumes of high-quality paired data for training, and their generalizability and interpretability remain active areas of research.

As noted in [13], in outdoor environments, metal patches on programmable metasurfaces are often blocked by particles such as snowflakes, ice, and both dry and damp sands. Such blockages can be categorized into two types, namely, partial blockage or complete blockage. Any types of blockages may lead to signal power loss which is usually represented by the amplitude attenuation coefficient. Ref. [13] stated that the amplitude attenuation coefficient is zero when the complete blockage happens. Otherwise, the amplitude attenuation coefficient is nonzero. In addition to the signal power loss, there is another type of failure, i.e., the phase error, for programmable metasurfaces. Usually, phase error is a random variable and can be assumed to follow a Gaussian distribution. Therefore, the overall fault will exhibit a Bernoulli-Gaussian (BG) distribution.

The model-based CS theory, an extension of the conventional CS theory, suggests that the inherent structure of the signal can also be leveraged to achieve stable recovery from compressive measurements [14]. In such a way, instead of relying on prior knowledge of the radiation pattern of the failure-free programmable metasurface to formulate the original problem into a sparse signal recovery one, we here directly take advantage of BG prior to ensure robust diagnostic performance when the measurements are limited. Specifically, a full probabilistic model representing such *a priori* information is established in the framework of Bayesian. Then, a low-complexity Bayesian inference strategy is implemented by combining variational expectation maximization (EM) algorithm and generalized approximate message passing (GAMP) technique.

* Corresponding author: Fang-Fang Wang (wangff@njupt.edu.cn).

Although the diagnostic technique with the BG prior reduces the necessary number of measurements without resorting to prior knowledge of the radiation pattern of the failure-free programmable metasurface, it still require measurements to be collected at multiple positions [15]. In this work, taking into account the dynamic tuning property of the programmable metasurface, its radiated fields are measured with a single fixed probe, thereby reducing the measurement time and avoiding potential errors due to probe movement.

In our earlier work, the concept of BG prior was first used for high-frequency electromagnetic imaging of metallic reflectors [16] and then introduced into the regular array failure diagnosis [17]. However, the differential strategy and multi-position measurement procedure were required in our previously proposed array failure diagnosis method. Besides, our previous work only considered the case of on-off faults. In this paper, the BG prior is directly incorporated into the failure diagnosis of programmable metasurfaces to avoid the differential strategy, and multi-position measurement process is not necessary in this work. Moreover, both amplitude attenuation and phase error due to malfunctioning are considered. As such, the technique proposed in this paper provides a powerful approach for onsite, high-efficiency, and high-accuracy diagnosis of programmable metasurfaces.

The remainder of this article is organized as follows. In Section 2, we briefly formulate the diagnostic problem of programmable metasurfaces. The proposed method is then introduced in Section 3. To verify the effectiveness of the proposed method, simulation results are provided in Section 4, followed by conclusions in Section 5.

2. MATHEMATICAL FORMULATION

As shown in Fig. 1, let us consider a programmable metasurface composed of M uniformly spaced resonant elements along the x-axis and N uniformly spaced resonant elements along the y-axis. Then, the total number of resonant elements is $L = M \times N$. For a specific coding configuration, the far-field measured at a fixed observation point P can be expressed as [18]

$$y_k = \sum_m \sum_n b_{mn} e^{j\Delta\varphi_{mn}}$$

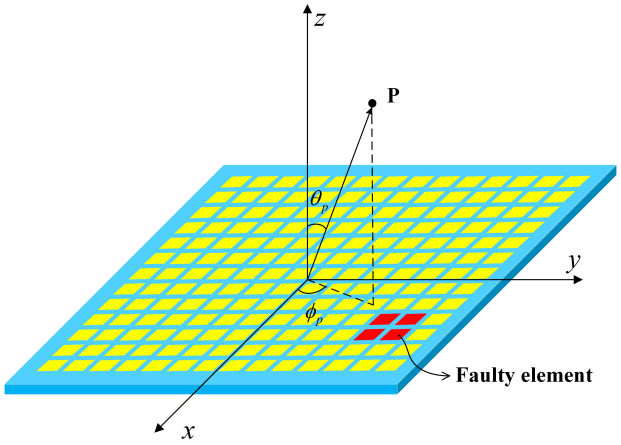

FIGURE 1. Geometry of the programmable metasurface.

$$e^{j\left\{\varphi_{mn}^{(k)}+\beta\left(m-\frac{1}{2}\right)D\sin\theta_p\cos\phi_p+\beta\left(n-\frac{1}{2}\right)D\sin\theta_p\sin\phi_p\right\}} \quad (1)$$

where $0 \le b_{mn} \le 1$ represents the amplitude attenuation coefficient expressed as

$$b_{mn} = \begin{cases} \text{zero with probability } 1-\eta \\ \text{nonzero with probability } \eta \end{cases} \quad (2)$$

where $1-\eta$ is the probability that a complete blockage happens. And, $-\pi \le \Delta\varphi_{mn} \le \pi$ denotes the phase error due to malfunctioning. Besides, θ_p and ϕ_p are the elevation and azimuth angles of the fixed observation point, respectively; D is the periodicity of the resonant elements, set to half the wavelength at the operating frequency; β is the wavenumber; and $\varphi_{mn}^{(k)}$ is the predesigned discrete phase response associated with the (m,n)th resonant element of the kth coding configuration.

While the half-wavelength periodicity suppresses mutual coupling and justifies its omission in our model, this effect may degrade performance in denser arrays. Therefore, developing methods to explicitly incorporate coupling effects represents a critical direction for future research.

Suppose that K coding configurations are performed and that the measurements at the fixed observation point are stacked into the vector $\tilde{\mathbf{y}} = [y_1, \cdots, y_K]^T$, then the signal model becomes

$$\tilde{\mathbf{y}} = \tilde{\mathbf{A}}\left(\tilde{\mathbf{b}} \odot \tilde{\mathbf{d}}\right) \quad (3)$$

where $\tilde{\mathbf{b}} = [b_{11}, \cdots, b_{MN}]^T$, $\tilde{\mathbf{d}} = [e^{j\Delta\varphi_{11}}, \cdots, e^{j\Delta\varphi_{MN}}]^T$, operator $\odot$ represents the Hadamard product, and $\tilde{\mathbf{A}}$ denotes the measurement matrix expressed as

$$\tilde{\mathbf{A}} = \begin{bmatrix} e^{j\left\{\varphi_{11}^{(1)}+c_{11}\right\}} & \cdots & e^{j\left\{\varphi_{MN}^{(1)}+c_{MN}\right\}} \\ \vdots & \ddots & \vdots \\ e^{j\left\{\varphi_{11}^{(K)}+c_{11}\right\}} & \cdots & e^{j\left\{\varphi_{MN}^{(K)}+c_{MN}\right\}} \end{bmatrix} \quad (4)$$

with

$$\begin{aligned} c_{mn} &= \beta\left(m-\frac{1}{2}\right)D\sin\theta_p\cos\phi_p \\ &\quad +\beta\left(n-\frac{1}{2}\right)D\sin\theta_p\sin\phi_p. \end{aligned} \quad (5)$$

Since matrix $\tilde{\mathbf{A}}$, vector $\tilde{\mathbf{y}}$, and $\tilde{\mathbf{d}}$ are complex, separating the real part and imaginary part of them, Eq. (3) is converted to

$$\mathbf{y} = \mathbf{A}\mathbf{x} \quad (6)$$

with

$$\mathbf{x} = \mathbf{b} \odot \mathbf{d} \quad (7)$$

$$\mathbf{b} = \begin{bmatrix} \tilde{\mathbf{b}} \\ \tilde{\mathbf{b}} \end{bmatrix} \quad (8)$$

$$\mathbf{d} = \begin{bmatrix} \mathrm{Re}(\tilde{\mathbf{d}}) \\ \mathrm{Im}(\tilde{\mathbf{d}}) \end{bmatrix} \quad (9)$$

$$\mathbf{A} = \begin{bmatrix} \mathrm{Re}(\tilde{\mathbf{A}}) & -\mathrm{Im}(\tilde{\mathbf{A}}) \\ \mathrm{Im}(\tilde{\mathbf{A}}) & \mathrm{Re}(\tilde{\mathbf{A}}) \end{bmatrix} \tag{10}$$

$$\mathbf{y} = \begin{bmatrix} \mathrm{Re}(\tilde{\mathbf{y}}) \\ \mathrm{Im}(\tilde{\mathbf{y}}) \end{bmatrix} \tag{11}$$

where $\mathrm{Re}(\cdot)$ and $\mathrm{Im}(\cdot)$ represent operators that return the real and imaginary parts, respectively.

Obviously, the goal of the diagnostics procedure is to reconstruct $\mathbf{x}$ by inverting the linear model (6). In practice, however, we want to make as few measurements as possible. Besides, the number of independent radiation patterns, and hence measurement information is also limited due to the finite Q-factor of the programmable metasurface. In such a case, the linear inversion for failure diagnosis of programmable metasurfaces is ill-posed.

3. METHODOLOGY

It is well known that using *a priori* knowledge of the unknowns can compensate for the lack of measurement information, thereby overcoming the ill-posedness of the linear inverse problem. Since the amplitude attenuation coefficient b_{mn} can be expressed as Eq. (2), and the phase error $\Delta\varphi_{mn}$ usually follows a Gaussian distribution, each entry of $\mathbf{x}$ will follow the BG distribution. In those circumstances, an inversion method which exploits such *a priori* information will be used in this work to deal with the inherent ill-posedness in the failure diagnosis of programmable metasurfaces. A brief description of this method is given below.

3.1. Bayesian Model

Similar to the conventional sparse Bayesian learning (SBL) framework [19, 20], a prior model is first constructed, i.e.,

$$p(\mathbf{x}) = \prod_l (1-\eta)\delta(x_l) + \eta N(x_l; \mu, \nu) \tag{12}$$

where $\delta(\cdot)$ represents the Dirac delta distribution, and μ and ν are the unknown mean and variance, respectively.

Typically, the measurement data is contaminated by additive white Gaussian noise (AWGN). Therefore, we can assume that the noise follows a Gaussian distribution with zero mean and unknown variance σ^2. Then, the likelihood function corresponding to the linear model (6) is expressed as

$$p(\mathbf{y} \mid \mathbf{x}) = N\left(\mathbf{y}; \mathbf{A}\mathbf{x}, \sigma^2\right). \tag{13}$$

3.2. EM-GAMP Framework for Bayesian Inference

In this subsection, a specialized Bayesian inference is derived. Firstly, in order to yield a computationally efficient Bayesian inference, the GAMP technique is employed to decouple the original likelihood function as

$$p(\mathbf{y} \mid \mathbf{x}) \approx \prod_l N(x_l; \hat{r}_l, \tau_l^r) \tag{14}$$

where $\hat{r}_l$ and τ_l^r are obtained through the GAMP algorithm. Let $\mathbf{z} = [z_1, \cdots, z_{2K}]^T = \mathbf{A}\mathbf{x}$ denote the noiseless output and its posterior can also be approximated using GAMP, i.e.,

$$p(\mathbf{z} \mid \mathbf{y}) \approx \prod_k p(y_k|z_k)\, N(z_k; \hat{p}_k, \tau_k^p) \tag{15}$$

where $\hat{p}_k$ and τ_k^p are also obtained through the GAMP algorithm. The GAMP is detailed in Algorithm 1, in which $j_{\max}$ stands for the maximum number of iterations of GAMP; $\mathbf{A}_{kl}$ is the (k,l)th entry of $\mathbf{A}$; $\hat{x}_l$ and τ_l^x represent the mean and variance of x_l; $\hat{z}_k$ and τ_k^z denote the mean and variance of z_k, respectively.

On the basis of the prior model (12) and decoupled likelihood function (14), the variational EM approach is then used to deduce the posterior distribution of $\mathbf{x}$, i.e.,

$$q(\mathbf{x}) \propto \exp\left(\langle \ln(p(\mathbf{x})p(\mathbf{y} \mid \mathbf{x}))\rangle\right) \tag{16}$$

where $\langle\cdot\rangle$ denotes the operator of the mathematical expectation. Also, the parameters $\{\eta, \mu, \nu, \sigma\}$ of the Bayesian model are updated in the variational EM algorithm, i.e.,

$$\{\eta, \mu, \nu, \sigma\} = \arg \max_{\{\eta,\mu,\nu,\sigma\}} \langle \ln(p(\mathbf{x})p(\mathbf{y} \mid \mathbf{x}))\rangle. \tag{17}$$

For simplicity, the posterior distribution of $\mathbf{x}$ and update rules for $\{\eta, \mu, \nu, \sigma\}$ are directly given by (details of the derivation can be found in [16])

$$q(\mathbf{x}) = \prod_l (1-\pi_l)\delta(x_l) + \pi_l N(x_l; \gamma_l, \upsilon_l) \tag{18}$$

with

$$\pi_l = \frac{1}{1 + \left(\frac{\eta}{1-\eta} \frac{N\left(\hat{r}_l; \mu, \tau_l^r + \nu\right)}{N\left(\hat{r}_l; 0, \tau_l^r\right)}\right)^{-1}} \tag{19}$$

$$\gamma_l = \frac{\hat{r}_l \nu + \tau_l^r \mu}{\tau_l^r + \nu} \tag{20}$$

$$\upsilon_l = \frac{\tau_l^r \nu}{\tau_l^r + \nu} \tag{21}$$

and

$$\eta = \frac{1}{2L} \sum_l \pi_l \tag{22}$$

$$\mu = \frac{1}{2\eta L} \sum_l \pi_l \gamma_l \tag{23}$$

$$\nu = \frac{1}{2\eta L} \sum_l \pi_l \left(|\mu - \gamma_l|^2 + \upsilon_l\right) \tag{24}$$

$$\sigma^2 = \frac{1}{2K} \sum_k \left(|y_k - \hat{z}_k|^2 + \tau_k^z\right). \tag{25}$$

Since the posterior distribution of $\mathbf{x}$ is obtained, which also follows the BG distribution, the mean and variance of each entry of $\mathbf{x}$ can be given by

$$\hat{x}_l = \pi_l \gamma_l \tag{26}$$

Algorithm 1: GAMP Algorithm

Input: $\mathbf{A}$, σ, $\hat{x}_l$, τ_l^x for $l = 1,\cdots,2L$

Initialize: $j = 0$, $\hat{s}_k(0) = 0$ for $k = 1,\cdots,2K$

While $j \le j_{\max}$ **do**

$j = j+1$

Compute $\tau_k^p(j) = \sum_l \mathbf{A}_{kl}^2 \tau_l^x$, $\hat{p}_k(j) = \sum_l \mathbf{A}_{kl}\hat{x}_l - \tau_k^p(j)\hat{s}_k(j-1)$

$$\hat{z}_k(j) = \frac{y_k\tau_k^p(j) + \sigma^2\hat{p}_k(j)}{\sigma^2 + \tau_k^p(j)},\ \tau_k^z(j) = \frac{\sigma^2\tau_k^p(j)}{\sigma^2 + \tau_k^p(j)}$$

$$\hat{s}_k(j) = \frac{\hat{z}_k(j) - \hat{p}_k(j)}{\tau_k^p(j)},\ \tau_k^s(j) = \frac{1 - \tau_k^z(j)/\tau_k^p(j)}{\tau_k^p(j)}$$

$$\tau_l^r(j) = (\sum_k \mathbf{A}_{kl}^2\tau_k^s(j))^{-1},\ \hat{r}_l(j) = \hat{x}_l + \tau_l^r(j)\sum_k \mathbf{A}_{kl}\hat{s}_k(j)$$

Output: $\hat{p}_k(j_{\max})$, $\tau_k^p(j_{\max})$, $\hat{z}_k(j_{\max})$, $\tau_k^z(j_{\max})$, $\hat{r}_l(j_{\max})$, $\tau_l^r(j_{\max})$ for $l = 1,\cdots,2L$ and $k = 1,\cdots,2K$

Algorithm 2: EM-GAMP framework for Bayesian inference

Initialize: $i = 0$, $\hat{x}_l(0) = 0$, $\tau_l^x(0) = 1$ $\sigma(0) = 1$, $\eta(0) = 0.5$, $\mu(0) = 0$, $\nu(0) = 1$

While $i \le i_{\max}$ **do**

$i = i+1$

Step1: Based on the values of $\hat{x}_l(i-1)$, $\tau_l^x(i-1)$, and $\sigma(i-1)$, call the GAMP algorithm to output $\hat{r}_l$, τ_l^r, $\hat{p}_k$, τ_k^p, $\hat{z}_k$, τ_k^z for $l = 1,\cdots,2L$ and $k = 1,\cdots,2K$.

Step2: Based on the outputs of the GAMP algorithm, compute $\pi_l(i)$, $\gamma_l(i)$, $\upsilon_l(i)$, $\eta(i)$, $\mu(i)$, $\nu(i)$, $\sigma(i)$ through (19), (20), (21), (22), (23), (24), and (25), then compute $\hat{x}_l(i)$ and $\tau_l^x(i)$ through (26) and (27).

Output: $\hat{x}_l(i_{\max})$, $\tau_l^x(i_{\max})$ for $l = 1,\cdots,2L$

$$\tau_l^x = \pi_l\left(\upsilon_l + (\gamma_l)^2\right) - (\pi_l)^2(\gamma_l)^2. \tag{27}$$

In summary, the whole Bayesian inference procedure iterates between the GAMP algorithm and variational EM algorithm. If the maximum number of iterations of EM (denoted as $i_{\max}$) is reached, the final result is output. This EM-GAMP framework for Bayesian inference is detailed in Algorithm 2. The computational complexity of this EM-GAMP framework is dominated by the GAMP algorithm. Thus, the total computational complexity of the EM-GAMP framework is $\mathcal{O}(i_{\max}j_{\max}KL)$.

4. NUMERICAL RESULTS

In this section, the performance of the proposed method which exploits the BG prior (referred to as the BG method) is evaluated and compared with that of the LS and CS methods. The Bayesian compressive sensing (BCS) as a traditional CS algorithm is applied in this work. Experiments are conducted on a 1-bit 20×20 programmable metasurface with the central frequency at 12.5 GHz [21]. Besides, the element periodicity is half of the wavelength corresponding to the central frequency, leading to $240 \times 240\,\text{mm}^2$ of the aperture. Faulty elements are assumed to be randomly distributed. Unless explicitly stated otherwise, the failure rate is set to 5%. In addition, the elevation and azimuth angles of the probe are fixed to $\theta_p = \pi/4$, $\phi_p = \pi/4$, respectively. In order to quantify the diagnostic performance, the relative model error (RME) is calculated as

$$\text{RME} = 10\log\left(\|\mathbf{x}' - \mathbf{x}\|_2^2 / \|\mathbf{x}\|_2^2\right) \tag{28}$$

where $\mathbf{x}'$ is the reconstructed vector.

We first evaluate the diagnostic performance of the three methods when the signal-to-noise ratio (SNR) is 50 dB and 15 dB, respectively. The qualitative results are shown in Figs. 2 and 3. Here, we define the compression ratio as the ratio of the number of measurements K to the total number of elements L and set it to 0.9 in this instance. In the figures, the squares outlined by red borders represent the faulty elements. At high SNR, the performance of the BG method closely aligns with that of the BCS method and is superior to that of the LS method. At low SNR, the diagnostic accuracy of the proposed method is much higher than the others.

Table 1 lists the RMEs corresponding to Fig. 2 and Fig. 3. It can also be concluded that the proposed method has higher diagnostic accuracy regardless of whether the SNR is high or low. Fig. 4 displays the curves of the RMEs computed by LS, BCS, and BG across various SNRs ranging from 5 dB to 60 dB. With the increase of SNR, the RMEs of all three methods decrease. Furthermore, at different noise levels, RMEs of the BG method consistently outperform those of the LS and BCS methods, demonstrating its superior performance.

TABLE 1. RMEs corresponding to Figs. 2 and 3.

	LS	BCS	BG
50 dB	−10.0823	−29.6885	**−49.2763**
15 dB	−4.3406	−2.2300	**−17.9361**

To study the impact of the number of measurements on the performance of the diagnostic method, RMEs of the BG method, LS method, and BCS method are calculated with different compression ratios as shown in Fig. 5, the RME curves have a steep drop and then tend to be stable. The steep drop occurs earlier for the proposed BG method, which indicates that this method can achieve the desired diagnostic accuracy with fewer measurements. As an example, Fig. 6 displays diagnostic results of the three methods with compression ratio $K/L = 0.5$.

It is noted that the proposed diagnostic method maintains 100% accuracy despite imperfect parameter estimation under low SNR or compression ratios. This performance is achieved by a decision-making step: a meta-atom is classified as faulty only if its recovered amplitude attenuation or phase error surpasses a predefined tolerance threshold.

To test the impact of the number of faults on the performance of the diagnostic method, we plot the RME against failure rate (i.e., the ratio of the number of faults to the total number of elements), while keeping an SNR of 50 dB and a compression ratio of 0.9 or 0.5. Here, a comparison is also made with existing programmable metasurface diagnostic methods, such as

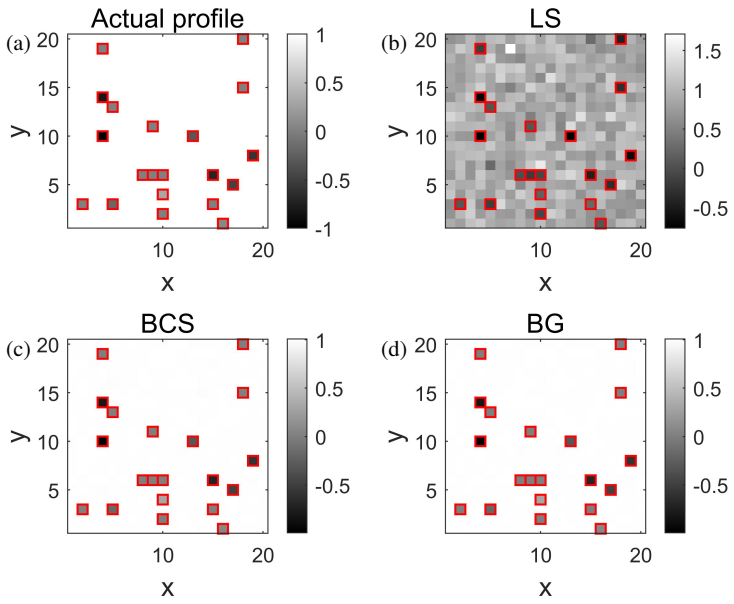

FIGURE 2. Actual profile and diagnosis results with compression ratio $K/L = 0.9$ and SNR $= 50$ dB. (a) Actual profile, (b) LS, (c) BCS, (d) BG.

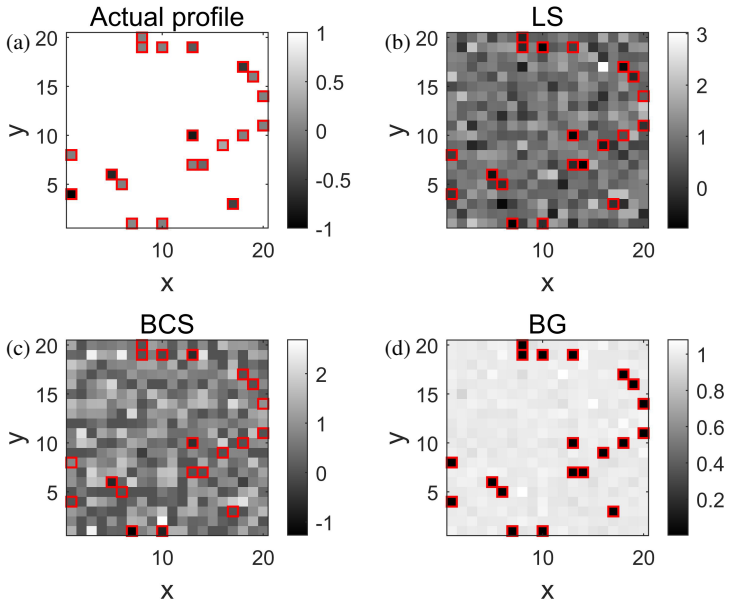

FIGURE 3. Actual profile and diagnosis results with compression ratio $K/L = 0.9$ and SNR $= 15$ dB. (a) Actual profile, (b) LS, (c) BCS, (d) BG.

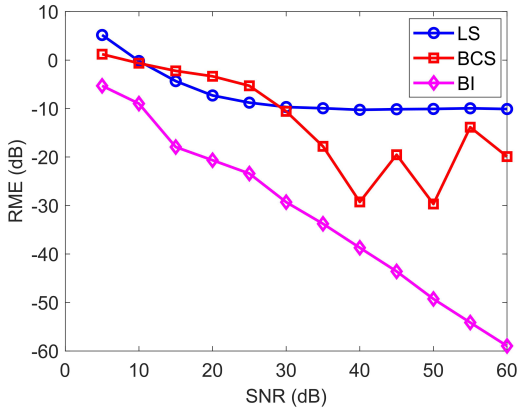

FIGURE 4. RME versus SNR.

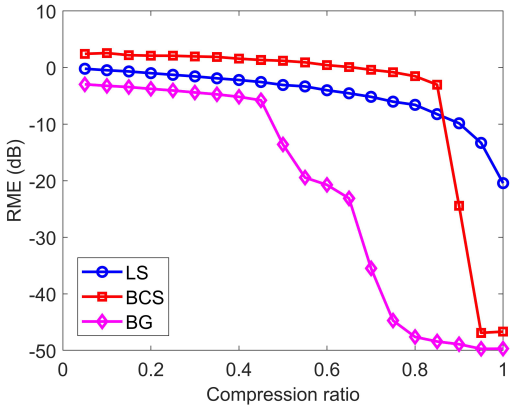

FIGURE 5. RME versus compression ratio K/L.

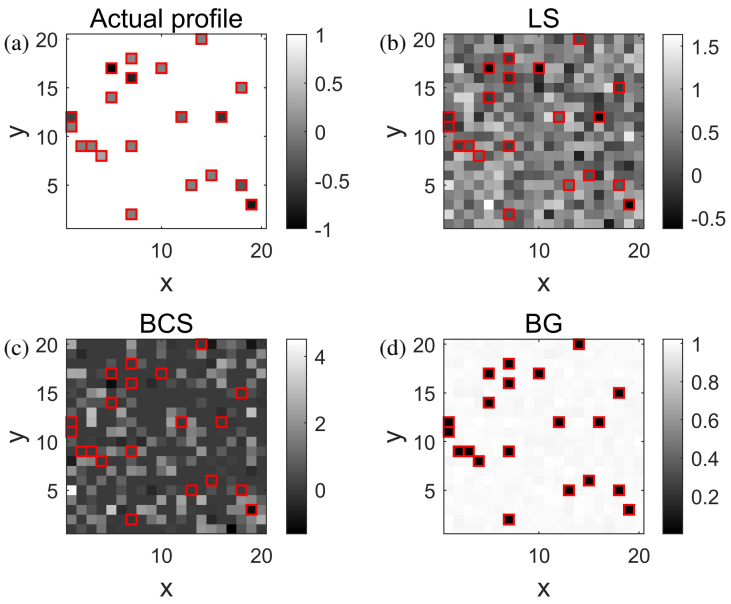

FIGURE 6. Actual profile and diagnosis results with compression ratio $K/L = 0.5$. (a) Actual profile, (b) LS, (c) BCS, (d) BG.

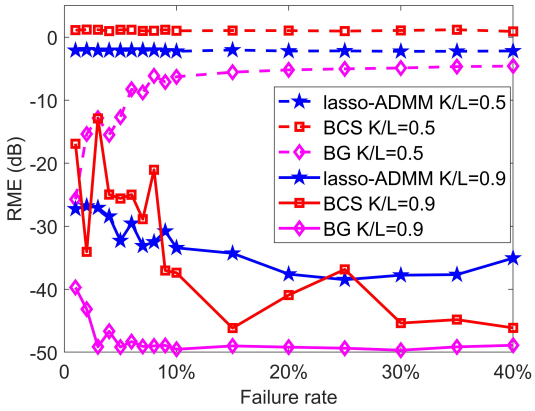

FIGURE 7. RME versus failure rate.

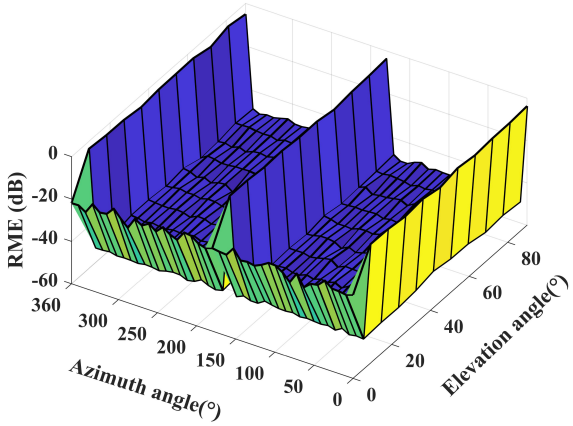

FIGURE 8. Influence of the probe position on the diagnostic result of the proposed method.

lasso-ADMM [7]. Since the LS method does not yield an acceptable result, we will no longer show its results.

As shown in Fig. 7, with $K/L = 0.9$, all three methods are robust against the number of faulty elements, while the proposed BG method achieves the minimal diagnostic errors at any failure rate. With $K/L = 0.5$, the performance of BCS and lasso-ADMM is severely degraded, while the proposed method is still feasible at low failure rates. Compared with the results in [11], we find that the robustness against the number of faulty elements of our proposed method is not as good as that of the conjugate gradient complex soft threshold (CG-CST) algorithm. However, the computational complexity of each iteration of CG-CST is $\mathcal{O}(KL^3)$. For large L, this is far greater than $\mathcal{O}(j_{\max}KL)$, the complexity of one iteration of our proposed method.

The effect of the choice of the probe position is also discussed. Some researchers have pointed out that the closer the probe is to the main lobe of the array antenna beam, the higher the diagnostic accuracy is, while for programmable metasurfaces, as stated in [22], the far-field pattern of a random coding configuration is also randomly distributed. Therefore, the choice of the probe position usually does not affect the diagnosis of the programmable metasurface. However, the performance of the proposed method is related to the measurement matrix. When the azimuth angle of the probe is set to 0 or π, the randomness or independence of the measurement matrix may not be satisfied, resulting in the deterioration of the diagnostic performance of the proposed method. The simulation results of the proposed method under different probe positions are shown in Fig. 8, which proves this point.

Last, we compare the diagnostic performances of the BG method with and without the differential strategy. In this paper, our aim is only to locate the faulty elements. As a consequence, the results presented in Fig. 9 prove that the BG method yields similar diagnostic performance at noise levels higher than 15 dB whether the differential strategy is used or not. In addition, as illustrated in Fig. 10, while the differential strategy is advantageous in reducing the compression ratio, the

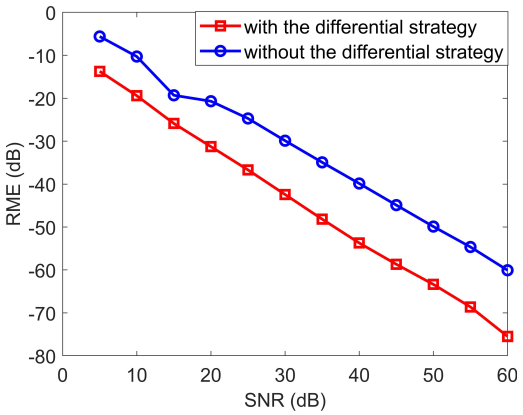

FIGURE 9. RMEs of the BG method at different noise levels with and without the differential strategy.

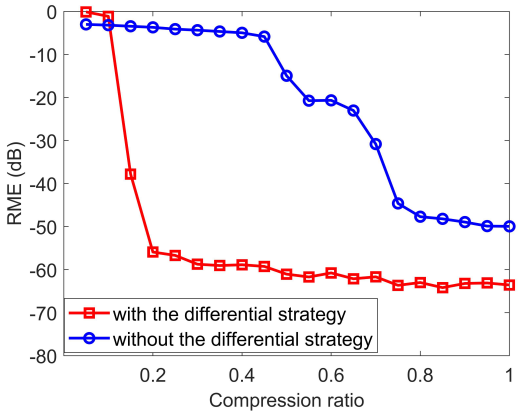

FIGURE 10. RMEs of the BG method at different compression ratios with and without the differential strategy.

BG method can still achieve a compression ratio of 0.5 even without utilizing the differential strategy.

5. CONCLUSION

This paper proposes a new method for detecting failures of programmable metasurfaces by combining a single-point measurement strategy and a BG prior. Leveraging the single-point measurement strategy has led to significant reductions in both measurement time and error. In addition, the utilization of the BG prior has effectively addressed the ill-posedness of the failure diagnosis problem, thus achieving a low compression ratio without relying on prior knowledge of the radiation pattern of the failure-free programmable metasurface. The proposed approach also exhibits high accuracy and has good robustness against noise, probe position, and failure rate.

In fact, programmable metasurfaces are usually large, and hence the measurements of their patterns will probably happen in the near field. Besides, real-world systems exhibit additional complexities and uncertainties that are not fully captured in our simulations. Bridging the gap between simulation and reality will pave the way for successful implementation of the proposed method in real-world scenarios. Thus, measurement verification will be conducted in the future to further identify potential challenges or limitations of our proposed method.

ACKNOWLEDGEMENT

This work was supported in part by the National Natural Science Foundation of China under Grant 62471250 and in part by the Natural Science Foundation of Nanjing University of Posts and Telecommunications under Grant NY223089.

REFERENCES

[1] Hu, S., M. Li, J. Xu, H. Zhang, S. Zhang, T. J. Cui, P. del Hougne, and L. Li, "Electromagnetic metamaterial agent," *Light: Science & Applications*, Vol. 14, No. 1, 12, 2025.

[2] Ma, Q., Q. Xiao, Q. R. Hong, X. Gao, V. Galdi, and T. J. Cui, "Digital coding metasurfaces: From theory to applications," *IEEE Antennas and Propagation Magazine*, Vol. 64, No. 4, 96–109, Aug. 2022.

[3] Nourinovin, S., M. Navarro-Cía, M. M. Rahman, M. P. Philpott, Q. H. Abbasi, and A. Alomainy, "Terahertz metastructures for noninvasive biomedical sensing and characterization in future health care [Bioelectromagnetics]," *IEEE Antennas and Propagation Magazine*, Vol. 64, No. 2, 60–70, Apr. 2022.

[4] Zhao, H., S. Hu, H. Zhang, Z. Wang, H. Dong, P. del Hougne, T. J. Cui, and L. Li, "Intelligent indoor metasurface robotics," *National Science Review*, Vol. 10, No. 8, nwac266, 2023.

[5] Bai, G., C. Liao, Y. Liu, and Y.-F. Cheng, "Far-field phaseless diagnosis for impaired arrays based on artificial neural networks and compressed sensing," *IEEE Transactions on Antennas and Propagation*, Vol. 72, No. 2, 1581–1592, Feb. 2024.

[6] Bai, G., C. Liao, Y. Liu, and Y.-F. Cheng, "Rapid failure diagnosis of impaired linear antenna arrays based on matrix pencil method," *IEEE Antennas and Wireless Propagation Letters*, Vol. 21, No. 8, 1708–1712, Aug. 2022.

[7] Palmeri, R., G. M. Battaglia, A. F. Morabito, S. Costanzo, F. Venneri, and T. Isernia, "Fault diagnosis of realistic arrays from a reduced number of phaseless near-field measurements," *IEEE Transactions on Antennas and Propagation*, Vol. 71, No. 9, 7206–7219, Sep. 2023.

[8] Sun, W., Y. Zhang, and H. Zhao, "A fast failure diagnosis method of planar arrays from far-field samples," *IEEE Antennas and Wireless Propagation Letters*, Vol. 23, No. 6, 1769–1773, Jun. 2024.

[9] Wang, F.-F., K.-M. Li, Y. Mao, and Q. H. Liu, "A hybrid born iterative method for diagnosis of planar arrays with amplitude-only far-field measurements," *IEEE Antennas and Wireless Propagation Letters*, Vol. 23, No. 2, 548–552, Feb. 2024.

[10] Li, L., R. Ying, Y. Li, L. He, and P. S. R. Diniz, "RIS array diagnosis for mmWave communication systems," *IEEE Signal Processing Letters*, Vol. 31, 1980–1984, 2024.

[11] Prajosh, K. P., F. Ferranti, and U. K. Khankhoje, "Reference-free fault diagnosis and corrected field prediction in a planar antenna array," *IEEE Antennas and Wireless Propagation Letters*, Vol. 23, No. 2, 743–747, Feb. 2024.

[12] Bai, G., C. Liao, Y. Liu, L. Zhao, X. Zhong, and Y. F. Cheng, "Knowledge-based conditional generative adversarial network for conformal antenna array diagnosis," *IEEE Antennas and Wireless Propagation Letters*, Vol. 23, No. 36, 1744–1748, Jun. 2024.

[13] Eltayeb, M. E., T. Y. Al-Naffouri, and R. W. Heath, "Compressive sensing for millimeter wave antenna array diagnosis," *IEEE Transactions on Communications*, Vol. 66, No. 6, 2708–2721,

Jun. 2018.

[14] Baraniuk, R. G., V. Cevher, M. F. Duarte, and C. Hegde, "Model-based compressive sensing," *IEEE Transactions on Information Theory*, Vol. 56, No. 4, 1982–2001, Apr. 2010.

[15] Xiong, C., G. Xiao, Y. Hou, and M. Hameed, "A compressed sensing-based element failure diagnosis method for phased array antenna during beam steering," *IEEE Antennas and Wireless Propagation Letters*, Vol. 18, No. 9, 1756–1760, Sep. 2019.

[16] Wang, F.-F. and Q. H. Liu, "A Bernoulli-Gaussian binary inversion method for high-frequency electromagnetic imaging of metallic reflectors," *IEEE Transactions on Antennas and Propagation*, Vol. 68, No. 4, 3184–3193, Apr. 2020.

[17] Wang, F.-F., Y.-H. Xu, and Q. H. Liu, "Planar array diagnosis based on Bayesian learning with a Bernoulli-Gaussian prior model," *IEEE Transactions on Antennas and Propagation*, Vol. 70, No. 7, 6106–6110, Jul. 2022.

[18] Yao, H. M., M. Li, L. Jiang, K. L. Yeung, and M. Ng, "Antenna array diagnosis using a deep learning approach," *IEEE Transactions on Antennas and Propagation*, Vol. 72, No. 6, 5396–5401, Jun. 2024.

[19] Hansen, T. L., B. H. Fleury, and B. D. Rao, "Superfast line spectral estimation," *IEEE Transactions on Signal Processing*, Vol. 66, No. 10, 2511–2526, May 2018.

[20] Wu, Q., Y. D. Zhang, M. G. Amin, and B. Himed, "Multi-task Bayesian compressive sensing exploiting intra-task dependency," *IEEE Signal Processing Letters*, Vol. 22, No. 4, 430–434, Apr. 2015.

[21] Yang, H., F. Yang, S. Xu, Y. Mao, M. Li, X. Cao, and J. Gao, "A 1-bit 10×10 reconfigurable reflectarray antenna: Design, optimization, and experiment," *IEEE Transactions on Antennas and Propagation*, Vol. 64, No. 6, 2246–2254, Jun. 2016.

[22] Cui, T.-J., S. Liu, and L.-L. Li, "Information entropy of coding metasurface," *Light: Science & Applications*, Vol. 5, No. 11, e16172, 2016.